The influence on the oral bioavailability of solubilized and suspended drug in a lipid nanoparticle formulation : in vitro and in vivo evaluation

The influence on the oral bioavailability of solubilized and suspended drug in a lipid nanoparticle formulation: *in vitro* and *in vivo* evaluation

Kimberley Elbrink[a], Sofie Van Hees[a], Dirk Roelant[b], Tine Loomans[b], René Holm[c,d], Filip Kiekens[a]

[a] **University of Antwerp,** Department of Pharmaceutical Technology and Biopharmacy, Universiteitsplein 1, 2610 Wilrijk, Belgium, Kimberley.Elbrink@uantwerpen.be; Sofie.VanHees@uantwerpen.be
[b] **Janssen Pharmaceutica**, Discovery Sciences, DMPK, Turnhoutseweg 30, 2340 Beerse, Belgium, DROELANT@its.jnj.com; TLOOMANS@its.jnj.com
[c] **Janssen Pharmaceutica,** Drug Product and Development, Parenterals and Liquids, Turnhoutseweg 30, 2340 Beerse, Belgium, rholm@ITS.JNJ.com
[d] **University of Southern Denmark**, Department of Physics, Chemistry, and Pharmacy, Campusvej 55, 5230 Odense, Denmark, reho@sdu.dk

Corresponding author: Prof. dr. Filip Kiekens
Filip.Kiekens@uantwerpen.be
Tel.: +3232652687

Postal address: Universiteitsplein 1
Building A (A.015)
2610 Wilrijk Belgium

Abstract

The present study investigated the oral bioavailability of celecoxib when incorporated into solid lipid nanoparticles either dissolved or suspended. *In vitro* drug release in different media, *in vivo* performance, and *in vitro-in vivo* correlation were conducted. The results revealed that the compound was successfully encapsulated into the nanocarriers with good physicochemical properties for oral administration. The *in vitro* release profiles followed the Weibull model, with significant differences between the formulations containing the solubilized and the suspended compound. Furthermore, *in vitro* release data could be used to rank the observed *in vivo* bioavailability. The relative bioavailability of celecoxib from the solid lipid nanoparticles was 2.5- and 1.8-fold higher for the drug solubilized and suspended solid lipid nanoparticle formulation, respectively, when compared to the celecoxib reference. A significant difference was observed between the plasma concentration-time profiles and pharmacokinetic parameters for the three investigated formulations. Finally, this investigation displayed promising outcomes that both solubilized and suspended celecoxib in the lipid core of the solid lipid nanoparticles offers the potential to improve the compound's oral bioavailability and thereby reduce the dosing frequency.

Keywords

Solid lipid nanoparticles; Oral bioavailability; *In vitro-in vivo* correlation; Poorly water-soluble drugs; Celecoxib

1. Introduction

Oral drug delivery is the most preferred route of administration owing to the good patient convenience, resulting in great patient compliance. [1,2] However, many newly discovered drug molecules are poorly water-soluble with a high or low permeability, belonging to class II or IV, according to the biopharmaceutical classification system. The suboptimal biopharmaceutical properties of those compounds, such as low aqueous solubility, may result in a limited absorption after oral administration, and therefore a high clinical variation and potential failure. [3–5]

Lipid-based formulations have shown success to tackle these pharmaceutical issues for newly discovered drug molecules. [4] Those formulations are able to improve the oral bioavailability of lipophilic drugs owing to an increase of the solubility of the drug in the gastrointestinal tract, enhanced absorption, and potential prevention of the first-pass metabolism. [1,6] Among the lipid-based drug delivery systems, solid lipid nanoparticles have shown great potential as drug carriers because of their unique properties, including good physicochemical stability, good biocompatibility, nontoxicity and, controlled or sustained drug release. [7–9] Solid lipid nanoparticles are composed of a solid lipid matrix with entrapped drug molecules surrounded by a surfactant layer with good biocompatibility and biodegradability. [5,10–12] The lipid excipients and the digestion products of the lipids increase the drug solubility *in vivo* and play an important role in the formation of micelles. [1,13] Additionally, enhanced intestinal permeability of drugs, improved dissolution rate, and prolonged retention in the gastrointestinal tract contribute to a markedly improved drug oral bioavailability. [12,14,15]

During the past years, solid lipid nanoparticles have been explored for the delivery of poorly water-soluble drugs to improve oral bioavailability, e.g., simvastatin [12], sildenafil citrate [16], olmesartan medoxomil [17], and loperamide [10]. Usually, the compound of the lipid-based formulations is in a dissolved state in the lipid matrix, resulting in an avoidance of slow dissolution of the compound. Although several articles describe different drug/lipid ratio's with the compound into a solubilized state, a suspended state of the compound has to the best of our knowledge not been thoroughly investigated for solid lipid nanoparticles. [4,18]

For a full understanding of the lipid-based formulations, an in-depth characterization of the behavior of those nanocarriers by *in vitro* release, as well as *in vivo* release studies are necessary. [14,19] A different approach for the *in vitro* release of solid lipid nanoparticles than conventional solid dosage forms are needed, due to the excipients, which are not always soluble

in the release media. Therefore, the selection of the media for the *in vitro* drug release experiments is important to predict the *in vivo* drug release, to rank the oral bioavailability of the *in vivo* data, and obtain a good in *vitro-in vivo* correlation. [4,14,18]

In this study, a poorly water-soluble model compound, celecoxib, was used, belonging to class II of the biopharmaceutical classification system. The overall aim of this investigation was to determine if the oral bioavailability of the compound dosed in solid lipid nanoparticles could function equally when suspended versus solubilized in the lipid matrix. Other objectives of this investigation were: I) evaluation of the physicochemical properties of the formulations; II) to compare the *in vitro* release profiles of both formulations in different media; III) to assess the *in vivo* release profiles and pharmacokinetic parameters between the solubilized and suspended drug in the solid lipid nanoparticles; IV) to determine the influence of the lipid concentration on the oral bioavailability; and V) to investigate the *in vitro-in vivo* correlation.

2. Materials and Methods

2.1. Chemicals and reagents

Glyceryl monostearate pure (GMS), Tween® 80 extra pure, and sodium chloride were acquired from Carl Roth GmbH (Karlsruhe, Germany). Sodium deoxycholate was obtained from TCI Europe NV (Zwijndrecht, Belgium) and D-Lactose monohydrate was provided by Sigma-Aldrich Chemie GmbH (Schnelldorf, Germany). Celecoxib and Hydrochloric acid 37% were purchased from VWR (Leuven, Belgium). Sodium lauryl sulfate was bought from Fagron (Nazareth, Belgium). Acetonitrile HPLC grade and Methanol HPLC grade were obtained from Chem-lab Analytical BVBA (Zedelgem, Belgium). FeSSIF and FaSSIF were purchased from Fisher Scientific (Merelbeke, Belgium) and Pepsin powder from Acros Organics (Geel, Belgium). The water used in all experiments was ultrapure water from a Direct pure adept, Rephile Bioscience Ltd., Analis NV (Belgium).

2.2. Animals

Male Sprague Dawley rats were obtained from Charles River (Sulzfeld, Germany) with an age of 9-11 weeks and a bodyweight of 300 to 350 g. Animal Ethics Committee was in accordance with the local Belgium laws controlling the use of experimental animals and the EU Directive 2010/63/EU.

2.3. Methods

2.3.1. Saturated solubility of celecoxib in the lipid matrix

The saturated solubility of celecoxib in the lipid matrix was determined as described by Patel *et al.* [20]. In short, 5 g of the solid lipid, glyceryl monostearate, was transferred to a measuring cup at a temperature 5 to 10 degrees above the melting point of glyceryl monostearate (67°C ± 1°C). Thereafter, celecoxib was added in increments (approximately 5 mg) until the compound was dissolved. The maximum amount of drug dissolved in the lipid was determined in triplicate.

2.3.2. Preparation of the different formulations

2.3.2.1. Solid lipid nanoparticles

The solid lipid nanoparticles were produced as previously reported [21] using high-speed homogenization followed by ultrasonication. Briefly, the lipid phase (glyceryl monostearate) was kept in a molten state, 10 degrees above the melting point of the lipid (67°C ± 1°C), using a glass cell with water jacket connected to a circulating heating bath. The accurately weighed quantity of celecoxib was dispersed in the lipid phase. Subsequently, tween® 80 and sodium deoxycholate were dissolved in ultrapure water and heated until it became isothermal with the lipid phase. Afterwards, the lipid and aqueous phase were homogenized (IKA T18 digital UltraTurrax®, Staufen, Germany) at 8000 rpm for 5 minutes, while maintaining temperature with the aid of a thermal jacket around the sample holder of the homogenizer. The obtained oil in water emulsion was then quickly sonicated by a probe sonicator (Vibra-Cell VCX-750, Sonics, United States) for 1 minute at 20% amplitude. The hot nano-emulsion was cooled down in an icebox to accomplish solidification of the solid lipid to form solid lipid nanoparticles. The solid lipid nanoparticle dispersions were stored overnight at -20°C and lyophilized for 96 hours in a FreeZone 1 Liter Benchtop Freeze Dry System (Model 7740030) (Labconco, MO, USA) with 5% (w/w) D-Lactose monohydrate as a cryoprotectant. [22–24] **Table 1** shows the composition of the different formulations. Formulation CCX-1 contained the maximum amount of drug that could be solubilized in the lipid, while formulation CCX-2 contained approximately five times more drug than the CCX-1 formulation.

2.3.2.2. Celecoxib reference formulation for the in vivo study

The celecoxib reference (CCX-3) was a submicron oil in water emulsion produced by high-speed stirring followed by ultrasonication. Celecoxib (3 mg/g), soybean oil (0.2 g/g), and lecithin (0.012 g/g) were stirred until all components were dissolved at a temperature of 60°C. Meanwhile, glycerol (0.02 g/g) was mixed with ultrapure water (0.765 g/g) and heated to the

same temperature. Both phases were homogenized together at 24000 rpm for 5 min and subsequently sonicated with a probe sonicator for 5 min at 40% amplitude. The obtained lipid emulsion was kept at 4°C until further use.

2.3.3. Methods for analysis of celecoxib

2.3.3.1. Analytical method for the entrapment efficiency and *in vitro* release

The concentrations of celecoxib were measured by a HPLC-UV system (Shimadzu LC-20A, Tokyo, Japan) equipped with a pump (Shimadzu LC-20AT), an auto-sampler (Shimadzu SIL-20A), a degasser (DGU-20A5), and a diode-array detector (Shimadzu SPD-M20A). The mobile phase for celecoxib separation was composed of methanol and ultrapure water at a ratio of 75:25 and delivered over a reversed-phase C18 column (GraceSmart® RP18 Column 150 x 4.6 mm 5u 120A) at room temperature (25°C). The flow rate was set at 1 mL/min with an injection volume of 20 µL. The eluent was observed by UV detection at a wavelength of 250 nm. [25] Peak area integration was performed using LC Postrun Analysis (Shimadzu, Tokyo, Japan) and the drug concentration was determined with reference to an external calibration curve. This method was validated for linearity, accuracy, repeatability and intermediate precision.

2.3.3.2. Analytical method for biological samples

An accurate amount of plasma (10 µL) was stirred with 20 µL dimethyl sulfoxide, 20 µL water, and 200 µL acetonitrile and subsequently centrifuged for 20 min at 6000 x g at 5°C. The plasma concentrations of celecoxib were measured by UPLC chromatography (Waters Acquity UPLC system, Waters Corp., Milford, MA) connected to a tandem mass spectrometer (SCIEX API 4000 MS/MS system, Applied Biosystems, Carlsbad, CA) as previously described. [21] In short, the chromatographic separation was performed on a Acquity UPLC BEH C18 column (50 ×2.1 mm, 1.7 µm) from Waters Corp. (Milford, MA, USA). The mobile phase for the UPLC analysis consisted of 0.1% formic acid in water and acetonitrile (ACN) with a total run time of 1.7 min and at a flow rate of 0.60 mL/min. Gradient elution was carried out, started at 65:35 (V/V) water/acetonitrile and up to 2:98 (V/V) water/ACN at 1 min, afterwards, the column was cleaned with 98.0% ACN from 1.1 – 1.3 min. At 1.31 min, the mobile phase changed to 65:35 (V/V) water/acetonitrile till 1.7 min. The lower and upper limits of quantification obtained were 10 and 20000 ng/mL, respectively. The MS/MS detection had the following settings: Collision gas (CAD) 6.0, IS -4500 V, temperature (TEM) 550 °C, collision energy (CE) -30.0 V and entrance potential -10.0 V. A precursor-product ion transition from mass to charge ratio (m/z) of 380-316 was used for the detection of the compound.

2.3.4. Physicochemical characterization

2.3.4.1. Particle size distribution and zeta potential

Particle size distributions of unloaded and loaded solid lipid nanoparticles were determined by laser diffraction on a Mastersizer 3000 (Malvern, United Kingdom) using the wet dispersion method. The parameters were analyzed using the Mie theory. All measurements were performed in triplicate with number distribution as a result type. Results were expressed as the Dx(50), being the particle diameters accumulated number ratio of 50%.

The zeta potential of the samples was evaluated by dynamic light scattering using a Zetasizer Nano ZS (Malvern, United Kingdom), based on the Smoluchowski equation. The lyophilized solid lipid nanoparticles were re-dispersed in ultrapure water, diluted to a 2% (V/V) concentration with ultrapure water and placed in a disposable folded capillary cuvette. All analyses were carried out in triplicate at a temperature of 25°C. [26]

2.3.4.2. Entrapment efficiency and drug loading capacity

The entrapment efficiency (EE) and the drug loading capacity (LC) into the solid lipid nanoparticles were determined by measuring the concentration of the free drug from the solid lipid nanoparticles using the ultrafiltration-centrifugation technique. [27] The centrifugal filters (Merck Millipore, Belgium) had a 10-kD molecular weight cut-off membrane, made of regenerated cellulose. Firstly, the filters were washed with ultrapure water to hydrate the pores by centrifugation (3-16 PK, Sigma centrifuges, Germany) for 10 min at 14000 x g. Then, the solid lipid nanoparticle dispersions were diluted with ultrapure water to a concentration of 5 mg/mL to avoid blocking the membrane pores. Separation of the amount of free drug and the solid lipid nanoparticles was obtained by adding 500 µL of the diluted sample to the ultrafiltration filter tube and subsequently centrifuging for 30 min at 14000 x g. Afterwards the resultant percolate was diluted with methanol (ratio 1:1) and analyzed by high-performance liquid chromatography (HPLC). The entrapment efficiency and the drug loading capacity of the solid lipid nanoparticle formulations were calculated according to the following equations (Eq. (1) and Eq. (2)):

$$EE\ (\%) = \frac{W_T - W_F}{W_T} \times 100 \qquad \text{Eq. (1)}$$

$$LC\ (\%) = \frac{W_T - W_F}{W_{SLN}} \times 100 \qquad \text{Eq. (2)}$$

where W_T was the total amount of drug, W_F was the amount of free (not included) drug, and W_{SLN} was the total amount of solid lipid nanoparticles.

2.3.5. Solid-state characterization

Differential scanning calorimetry (DSC) analysis was performed using the Discovery DSC25 (TA Instrument, New Castle, DE, USA). Celecoxib, glyceryl monostearate, unloaded, and loaded solid lipid nanoparticles were accurately weighed in Tzero aluminum pans and crimp sealed. The enthalpy and temperature were calibrated by an indium standard and the heat capacity by a sapphire standard. A heating rate of 2°C/min with modulation of 1.6°C/min was applied in the range of -40°C to 200°C under nitrogen purge at a flow rate of 50 mL/min in a modulated temperature mode. The thermograms were directly obtained from the TA Instruments TRIOS software to determine and quantify the melting peak and were observed for crystallinity changes and compatibility of celecoxib with other excipients. Additionally, X-ray diffraction patterns of the lyophilized solid lipid nanoparticles and their solid components were explored by a PANalytical (Philips, Almelo, The Netherlands) X'PertPRO MPO diffractometer with a Cu LFF X-ray tube. Scanning of the samples was performed at 2θ range of 3° to 50°, at 45 kV operating voltage and 40 mA current with a step size of 0.02° and a step time of 500 sec/step.

2.3.6. *In vitro* drug release

The *in vitro* release profiles of drug-loaded solid lipid nanoparticles and celecoxib as such were studied in 200 mL release media of simulated gastric fluid (pH 1.2), fed state simulated intestinal fluid (pH 5), and fasted state simulated intestinal fluid (pH 6.5) using a modified USP apparatus 2 at 37 ± 1°C for 24 h. [28] Sodium lauryl sulfate (1% (w/V)) was added to all release media as a solubilizing agent to maintain sink conditions. Aliquots (1 mL) were withdrawn at specified time intervals (2, 5, 10, 15, 30, and 45 min, and 1, 1.5, 2, 3, 4, 6, 8, and 24 h), and replaced by an equal volume of fresh release medium to maintain a constant volume. Subsequently, the collected samples were centrifuged for 30 min at 21460 x g. The drug concentration in the supernatants was determined by HPLC, as described above. All experiments were performed in triplicate, and the results were expressed in mean values ± SD. The *in vitro* release data were fitted into first-order, Higuchi and Weibull models for evaluation of the drug release phenomena by the spreadsheet-based nonlinear analysis as described by Juhász et al. [29] The determination coefficient (R^2) was calculated to compare the non-linear mathematical models. [29–31]

2.3.7. *In vivo* drug release

2.3.7.1. Animal study

The animals were retained in polysulphone cages with corn hub bedding material and were kept in controlled rooms with a temperature of 20-24°C, a light cycle of 12 h, and a humidity of 30-70%. Seven days before the start of the study, the rats were acclimatized and had access to food and water ad libitum. After acclimatization, the 18 male rats were randomly allocated into three groups (n = 6 for each group). Group 1 and group 2 received once 5 mL/kg solid lipid nanoparticles, namely CCX-1, and CCX-2, and rats of group 3 were dosed once 5 mL/kg with the celecoxib reference (CCX-3). All formulations had a concentration of 3 mg/mL of celecoxib and were orally administered once on day 1 of the study.

2.3.7.2. Blood sample collection and plasma preparation

Blood samples were withdrawn from the tail vein of the rats and 32 µL of the blood sample was collected in Vitrex micro hematocrit tubes at designated intervals of time ranging from 0.5 h to 30 h hours post oral administration. After sampling, blood samples were immediately placed on ice and centrifuged for 10 min at 5°C and 1500 x g. Subsequently, plasma aliquots (10 µL) were collected with Vitrex end-to-end pipettes in FluidX tubes and stored in the freezer until further analysis.

2.3.7.3. *In vitro-in vivo* correlations

The correlation of *in vitro* release tests with *in vivo* data is presumably the best for class II drugs (low solubility and high permeability) of the biopharmaceutical classification system because the dissolution rate is the primary limiting aspect of the absorption. [32] This correlation can be mathematically treated by system analysis. [33] The plasma concentration-time profile after intravenous administration of celecoxib, as described by Elbrink et al. [21], was defined as the weighting function *W(t)*. The plasma concentration profile obtained after oral administration of the solid lipid nanoparticles can be treated as the response function *R(t)* of the system. The input function *I(t)* can be described by deconvolution. [34,35] The "area-area-points" method is the most flexible and general, where the response function is taken as points of the true curve and the input and weighting functions are construed by "staircase" curves. [33] As described by Langenbucher [33], numerical deconvolution was used according to the following sum (Eq. (3)):

$$I\ (x_i) = \frac{[R(t)/T - \sum_{k=1}^{n} I(x_k) * W(x_{n-k+1})]}{W(x_i)} \qquad \text{Eq. (3)}$$

where $W(x_k)$ and $I(x_k)$ are the average weight and input rate between the times x_{k-1} and x_k, and T is the time interval. The numerical deconvolution was based on the obtained plasma concentration-time profiles.

2.3.7.4. Pharmacokinetic parameters and statistical analysis

The pharmacokinetic parameters including the maximum drug concentration observed in plasma (C_{max}), the area under the curve (AUC), the time to reach the maximum concentration (T_{max}), the terminal half-life ($T_{1/2}$), and the mean residence time (MRT) were determined by non-compartmental analysis (PKSolver®; Microsoft Excel). All the determined values were expressed as mean ± SD. Statistical analyses were performed using the Statistical Package for Social Sciences (SPSS ver. 27.0) using a two-way ANOVA.

2.3.8. Stability study

The stability of the lyophilized celecoxib-loaded solid lipid nanoparticles was studied according to the International Conference on Harmonization (ICH) Q1A (R2) guidelines. [36] The two formulations (n = 3) were stored in glass vials at 4 ± 2 °C for three months. The storage stability of the solid lipid nanoparticles was evaluated by particle size, zeta potential, and entrapment efficiency at 0, 1, and 3 months. Statistical evaluation was performed using SPSS ver. 27.0.

3. Results and discussion

3.1. Physicochemical characterization of the solid lipid nanoparticles

The saturated solubility of celecoxib in glyceryl monostearate was found to be 41.1 mg/g. Hence, the CCX-1 formulation consisted of the maximum amount of celecoxib (± 4% (w/w) drug relative to lipid) that could be solubilized in the lipid, whereas the CCX-2 formulation was supersaturated with celecoxib (± 20% (w/w) drug relative to lipid). After the production of the SLN formulations, they were characterized for their particle size (Dx(50)), zeta potential (ZP), entrapment efficiency (EE), and drug loading capacity (LC) (**Table 2**).

The average particle size of the drug-free and drug-loaded solid lipid nanoparticles ranged from 19.67 to 91.47 nm with span indices of the formulations around 1.3. The celecoxib-loaded solid lipid nanoparticles had a slightly increased particle size relative to the drug-free solid lipid nanoparticles. According to the statistical analyses, a significant size difference was observed between the CCX-1 and CCX-2 formulation (p=0.000), which can possibly be explained by the drug to lipid ratio. The higher the drug to lipid ratio, the larger the solid lipid nanoparticles are.

[37] Importantly, a particle size <300 nm is a crucial factor for the gastrointestinal absorption of the solid lipid nanoparticles after oral administration. [7,8,12,17]

The zeta potential of all formulations had a negative value (attributed to the anionic nature of sodium deoxycholate) around -45 mV, indicating the stability against aggregation of the solid lipid nanoparticles due to electrostatic repulsion among the particles with a similar charge. [26,38] No significant differences were recognized between the zeta potential of the blanco, CCX-1, and CCX-2 formulations, suggesting there was not an actual 'electrical charge' difference present. So, the surface charge was not influenced by the incorporation of celecoxib in the solid lipid nanoparticles.

The celecoxib-loaded solid lipid nanoparticles presented high entrapment efficiency (>90%), which was significantly different between the two formulations with a low and high drug to lipid ratio ($p=0.004$). The high levels of entrapment efficiency may be due to the lipophilic nature of celecoxib (logP = 3.5) [39], resulting in a higher affinity for the solid lipid matrix. [40,41] The average drug loading capacity for the CCX-2 formulation (19.79%) was approximately five times higher than for the CCX-1 formulation (3.88%). High loading capacity is essential for diminishing the volume of the final dosage form. [11,42]

3.2. Solid-state characterization of the solid lipid nanoparticles

Interpretation of the crystallinity and interaction among celecoxib and the lipid matrix was investigated by monitoring the freeze-dried solid lipid nanoparticles, pure celecoxib, and glyceryl monostearate (**Fig. 1A**). Pure celecoxib and glyceryl monostearate demonstrated a sharp endothermic peak at 161.66°C and 53.69°C, corresponding to their melting points of the crystalline forms. [43] The drug-free and drug-loaded solid lipid nanoparticles exhibited no comparable peak of pure celecoxib, suggesting that the drug was in a non-crystalline state within the lipid matrix of the solid lipid nanoparticles. The thermograms of the SLN formulations showed a slight shift and broadening of the endothermic peak of glyceryl monostearate to a lower temperature. These findings can possibly be explained by the lipid-surfactant interactions and the Kelvin effect (small particle size). [44] Noteworthy, enhanced water solubility and oral bioavailability is assumed due to the conversion of crystalline celecoxib to an amorphous state.

The crystal lattice arrangements were evaluated by X-ray powder diffraction. **Fig. 1B** presents the X-ray diffraction patterns of drug-free and drug-loaded solid lipid nanoparticles, as well as pure celecoxib and glyceryl monostearate. The sharp indicative peaks of pure celecoxib at 2-

theta between 15° and 30° indicated the crystalline nature of the drug. [45] These sharp peaks disappeared in the diffractogram of the CCX-1 formulation, suggesting that celecoxib was solubilized upon incorporation into the lipid matrix, as suggested by the solubility data describe above. However, the XRD pattern of the CCX-2 formulation presented some peaks with a reduced intensity that could be related to the presence of celecoxib, due to the high drug to lipid ratio. Additionally, crystalline peaks of plain glyceryl monostearate were observed at 2-theta between 18° and 25° (β-form). [46,47] The intensity of those peaks was reduced in the drug-free and drug-loaded solid lipid nanoparticles, resulting in a less ordered crystal arrangement of the lipid matrix, which could be a reason for the higher drug incorporation. [12,48] In conclusion, the DSC thermograms and XRD patterns were in good agreement, implying a fully solubilized and amorphous state of celecoxib for the CCX-1 formulation and a partially amorphous state for the CCX-2 formulation. The release of celecoxib from the solid lipid nanoparticles was influenced by the adjustments in crystallinity of the drug and solid lipid. [49]

3.3. *In vitro* drug release

The *in vitro* release profiles of celecoxib from the SLN formulations and celecoxib as such were evaluated in SGF, FeSSIF, and FaSSIF at body temperature (37 ± 1 °C) for 24 hours. Owing to its poor aqueous solubility, sodium lauryl sulfate (1%, w/V) was added to the release media as a solubilizing agent. The results of the cumulative drug release are depicted in **Fig. 2** and **Fig. 3**. **Fig. 2** shows the release profiles of the two different formulations and pure celecoxib per formulation in three different media, while **Fig. 3** presents the release patterns per medium.

Comparing the graphs per formulation (**Fig. 2**), a similar biphasic release profile was observed with an initial fast release followed by a slow release. The burst release of celecoxib from the solid lipid nanoparticles may be due to the presence of celecoxib attached to the outside or in the outer shell layer of the solid lipid nanoparticles. Followed by a phase of slow celecoxib release, which referred to the degradation of the solid lipid matrix and the diffusion of the incorporated drug from the nanoparticles due to the strong drug-lipid interactions as indicated by the solid-state characterization. Glyceryl monostearate, the solid lipid, has a compact structure that does not grant the flow of the liquid phase, which ensures a slow release of celecoxib. [50] This final phase was not extended for hours. It could be suggested that this might be caused by the smaller particle size, which in turn creates a larger surface area for the drug-loaded solid lipid nanoparticles.

The CCX-1 formulation (**Fig. 2A**) had a faster release of celecoxib than the CCX-2 formulation (**Fig. 2B**), namely, 92% and 85% after 30 min. The drug release in the initial hour was influenced by the concentration of the lipid. CCX-1 had a higher lipid concentration and a lower drug to lipid ratio than the CCX-2 formulation, resulting in a faster drug release with increased lipid concentration. Another reason for the slower drug release may be due to the larger particle size of the CCX-2 solid lipid nanoparticles, which gives rise to a smaller surface area, and thus a reduction in drug diffusion. **Fig. 2C** shows the dissolution profile of pure celecoxib in the different media. Remarkably, celecoxib dissolved fastest in FeSSIF (pH 5), followed by FaSSIF (pH 6.5) and SGF (pH 1.2). This result may be described by the solubility of celecoxib. The celecoxib-loaded solid lipid nanoparticles exhibited a pH-dependent drug release. Celecoxib (pKa 11.1) has a net zero charge over the entire physiological pH. Therefore, celecoxib is more soluble in an alkaline than in an acidic environment. [51]

On the other hand, the results in **Fig. 3** present similar biphasic release profiles, as mentioned above. During the initial hour of drug release, a difference between the formulations was observed for each type of release medium. A general trend was recognized, in which the percentage of cumulative drug release was higher for the CCX-1 formulation than the CCX-2 formulation, followed by pure celecoxib. This observation was more pronounced in SGF (**Fig. 3A**) and FaSSIF (**Fig. 3C**) than in FeSSIF (**Fig. 3B**).

The obtained *in vitro* release data were fitted into the first-order, Higuchi and Weibull equations and the determination coefficient (R^2) was calculated. **Fig. 4** presents the R^2 values of the nonlinear models on different formulations in the three release media. Both the first-order and Weibull models demonstrated high determination coefficients (>0.9). Nevertheless, the Weibull equation fitted best to all the release data. The shape parameter (**Table 3**) was <1 for CCX and CCX-2, and >1 for CCX-1, respectively. [30,52]

Comparing the shape parameters between the different formulations and different media, it can be concluded that the CCX-1 formulation had a significantly different drug release profile than the CCX-2 formulation and pure celecoxib, whereas there was no significant difference between CCX-2 formulation and pure celecoxib. Another observation was the significant difference between the release of celecoxib in FeSSIF relative to FaSSIF and SGF. These results confirm the above-mentioned observations.

3.4. *In vivo* drug release

3.4.1. Pharmacokinetics

The average plasma concentration versus time profiles following single-dose administration of the SLN formulations and the reference are presented in **Fig. 5A**. The corresponding pharmacokinetic parameters are listed in **Table 4**. After oral administration of the SLN formulations and the celecoxib reference, a prominent initial burst release within the first 3 h was observed, indicating an amount of celecoxib on the outer shell layer of the nanoparticles, which was promptly exposed in the gastrointestinal tract, pursued by a fast absorption. [11,53] These findings were in line with the results of the *in vitro* release data as described above. As evidenced in **Fig. 5A**, the plasma concentrations of celecoxib were markedly higher for both SLN formulations compared to the celecoxib reference and ranked in the following order CCX-1 > CCX-2 > CCX-3.

The peak plasma concentration (C_{max}) of celecoxib of CCX-1 and CCX-2 formulations were 7107 ± 1134 ng/mL and 4283 ± 898 ng/mL, respectively, and were significantly higher than the celecoxib reference (2747 ± 168 ng/mL) ($p<0.05$). Similarly, a significant improvement in the area under the curve ($AUC_{0\rightarrow inf.}$) was determined upon the solid lipid nanoparticles administration compared to the reference. The $AUC_{0\rightarrow inf.}$ of the CCX-1 and CCX-2 were 2.5- and 1.8-fold higher than the CCX-3, suggesting a greater extent of oral absorption, an improved oral bioavailability, and overcoming the barriers that hinder the systemic availability. [11,12,54] Noteworthy, the time to reach peak plasma concentration (t_{max}) and the elimination half-life ($T_{1/2}$) were slightly delayed for the SLN formulations relative to the reference, although no significant effect was determined. This delay can possibly be explained by the presence of lipids in the duodenum, causing a delayed gastric emptying. [18,55] The mean residence time (MRT) was extended for the SLN formulations compared to the celecoxib reference, with a significant difference between the CCX-2 and CCX-3 ($p = 0.025$), but no significant difference between the CCX-1 and CCX-2 nor CCX-3 ($p>0.05$).

The relative bioavailability ($F_{resp.}$) was calculated by dividing the $AUC_{0\rightarrow inf.}$ of the SLN formulations by the $AUC_{0\rightarrow inf.}$ of the reference. The $F_{resp.}$ values were 249% and 181% for the CCX-1 and CCX-2 formulations, respectively, indicating that more celecoxib crossed the intestinal barrier than the celecoxib reference and supporting the hypothesis that the solid lipid nanoparticles significantly augmented the oral bioavailability as drug carriers.

As mentioned above, there was a clear difference between the plasma concentration-time profiles and pharmacokinetic parameters of CCX-1 and CCX-2. The CCX-2 formulation had a higher drug to lipid ratio and particle size compared to the CCX-1 formulation. Both factors affect the oral bioavailability of the drug encapsulated in solid lipid nanoparticles. The lower the drug to lipid ratio, the higher the lipid concentration in the formulation administered to the rats, leading to an increase in the bioavailability of celecoxib, as can be seen in **Table 4**. The smaller the particle size, the larger the surface area, leading to a more facile GI uptake by adhering to the gastrointestinal tract. [6,12,54,56]

Furthermore, tween 80 and sodium deoxycholate were used as surfactants in the preparation of the solid lipid nanoparticles. Both excipients are permeability enhancers, which enhance the permeability of the membrane. [5,8,41,54] Additionally, glyceryl monostearate was used as the lipid matrix of the solid lipid nanoparticles with more than 12-carbons chain length. Long-chain fatty acids enhance lymphatic uptake and diminish the first-pass effect of the drug. [6,15,50] Those mechanisms could assist, individually or together, for the improvement of the oral bioavailability of celecoxib from the nanocarriers.

3.4.2. *In vitro-in vivo* correlations

The deconvolution profiles of celecoxib based on the numerical deconvolution are presented in **Fig. 5B**. *In vitro-in vivo* correlation (IVIVC) can be determined to associate the *in vivo* absorption and the *in vitro* drug release for lipid nanoparticles. [57] In this research, the IVIVC was implemented to evaluate the absorption of celecoxib from different solid lipid nanoparticles and celecoxib reference. Specific time points for 10%, 50%, and 90% absorbed celecoxib were calculated to analyze the differences among the deconvolution profiles (**Table 5**). The CCX-3, CCX-1, and CCX-2 had a drug absorption of 50% after 2.3 h, 2.6 h, and 3.4 h, respectively. A similar trend was found for the time points of 10 and 90% of the drug absorption. Although, the data presented that the CCX-2 formulation tended to a higher extent of absorption relative to CCX-1 and CCX-3, no significant differences in the absorption of celecoxib between the three formulations were observed.

3.5. Stability study

The drug-free and drug-loaded solid lipid nanoparticles were monitored for three months on basis of zeta potential, particle size, and entrapment efficiency. The results of the storage stability at refrigerated temperature are presented in **Fig. A.1** and **Table A.1**. Looking at the results, no significant changes in any of the assessed parameters occurred. Noteworthy, a slight

455 increase in particle size (**Fig. A.1 (B)**) and decrease in entrapment efficiency (**Fig. A.1 (C)**)
456 could be determined, which can be due to aggregation and drug repulsion from the
457 nanoparticles, whereas no trend could be observed for the zeta potential. Overall, the solid lipid
458 nanoparticles were found to be stable for up to three months at refrigerated temperature.

459

460 ## 4. Conclusion

461 In summary, the model compound, celecoxib, was successfully incorporated into the solid lipid
462 nanoparticles with good physicochemical properties and stable up to three months at
463 refrigerated temperatures. The solid lipid nanoparticles of the CCX-1 formulation were
464 significantly smaller than those of the CCX-2 formulation due to the drug to lipid ratio.
465 Moreover, a significantly higher entrapment efficiency was observed for the CCX-2
466 formulation than for the CCX-1 formulation, while the zeta potential was not affected by the
467 incorporation of the compound. The solid-state characterization presented that the compound
468 was in an amorphous state in the solid lipid nanoparticles for the CCX-1 formulation and a
469 partially amorphous state for the CCX-2 formulation. The *in vitro* release showed a biphasic
470 release profile with an initial burst release followed by a slow release, following the Weibull
471 model. A trend could be observed where the CCX-1 formulation had a higher percentage of
472 cumulative drug release than the CCX-2 formulation, followed by pure celecoxib. To answer
473 the question posed in the introduction of the research article, both SLN formulations gave rise
474 to a significantly enhanced oral bioavailability of celecoxib in comparison with the drug
475 reference. The improvement of the oral bioavailability was more pronounced for the dissolved
476 (249%) than the suspended (181%) compound in the lipid matrix. Further, the *in vitro* drug
477 release data from the solid lipid nanoparticles were consistent with the *in vivo* results and could
478 be used to rank the *in vivo* oral bioavailability, namely CCX-1 > CCX-2 > CCX-3.

479

480 ## 5. Acknowledgments

481 The authors wish to thank everyone involved in this research. Furthermore, Abhishek Singh is
482 gratefully acknowledged for his expert help with the XRD patterns.

6. References

[1] N. Borkar, D. Xia, R. Holm, Y. Gan, A. Müllertz, M. Yang, H. Mu, Investigating the correlation between in vivo absorption and in vitro release of fenofibrate from lipid matrix particles in biorelevant medium, European Journal of Pharmaceutical Sciences. 51 (2014) 204–210. https://doi.org/10.1016/j.ejps.2013.09.022.

[2] C. Zhang, C. Gu, F. Peng, W. Liu, J. Wan, H. Xu, C.W. Lam, X. Yang, Preparation and optimization of triptolide-loaded solid lipid nanoparticles for oral delivery with reduced gastric irritation, Molecules. 18 (2013) 13340–13356. https://doi.org/10.3390/molecules181113340.

[3] M.A. Rahman, R.K. Harwansh, Z. Iqbal, Systematic Development of Sertraline Loaded Solid Lipid Nanoparticle (SLN) by Emulsification-Ultrasonication Method and Pharmacokinetic Study in Sprague-Dawley Rats, Pharmaceutical Nanotechnology. 7 (2019) 162–176. https://doi.org/10.2174/2211738507666190327145628.

[4] R. Holm, Bridging the gaps between academic research and industrial product developments of lipid-based formulations, Advanced Drug Delivery Reviews. 142 (2019) 118–127. https://doi.org/https://doi.org/10.1016/j.addr.2019.01.009.

[5] L. Hu, Q. Xing, J. Meng, C. Shang, Preparation and enhanced oral bioavailability of cryptotanshinone-loaded solid lipid nanoparticles, AAPS PharmSciTech. 11 (2010) 582–587. https://doi.org/10.1208/s12249-010-9410-3.

[6] N. Dudhipala, K.Y. Janga, Lipid nanoparticles of zaleplon for improved oral delivery by Box–Behnken design: optimization, in vitro and in vivo evaluation, Drug Development and Industrial Pharmacy. 43 (2017) 1205–1214. https://doi.org/10.1080/03639045.2017.1304957.

[7] B. Zhao, S. Gu, Y. Du, M. Shen, X. Liu, Y. Shen, Solid lipid nanoparticles as carriers for oral delivery of hydroxysafflor yellow A, International Journal of Pharmaceutics. 535 (2018) 164–171. https://doi.org/10.1016/j.ijpharm.2017.10.040.

[8] H. Hassan, R.O. Bello, S.K. Adam, E. Alias, M.M.R.M.M. Affandi, A.F. Shamsuddin, R. Basir, Acyclovir-loaded solid lipid nanoparticles: Optimization, characterization and evaluation of its pharmacokinetic profile, Nanomaterials. 10 (2020) 1–17. https://doi.org/10.3390/nano10091785.

[9] Z. Zhang, F. Gao, H. Bu, J. Xiao, Y. Li, Solid lipid nanoparticles loading candesartan cilexetil enhance oral bioavailability: In vitro characteristics and absorption mechanism in rats, Nanomedicine: Nanotechnology, Biology, and Medicine. 8 (2012) 740–747. https://doi.org/10.1016/j.nano.2011.08.016.

[10] L. Wei, Y. Yang, K. Shi, J. Wu, W. Zhao, J. Mo, Preparation and characterization of loperamide-loaded dynasan 114 solid lipid nanoparticles for increased oral absorption in the treatment of diarrhea, Frontiers in Pharmacology. 7 (2016) 1–9. https://doi.org/10.3389/fphar.2016.00332.

[11] O.S. Qureshi, H.S. Kim, A. Zeb, J.S. Choi, H.S. Kim, J.E. Kwon, M.S. Kim, J.H. Kang, C. Ryou, J.S. Park, J.K. Kim, Sustained release docetaxel-incorporated lipid nanoparticles with improved pharmacokinetics for oral and parenteral administration, Journal of Microencapsulation. 34 (2017) 250–261. https://doi.org/10.1080/02652048.2017.1337247.

[12] S.Z.H. Rizvi, F.A. Shah, N. Khan, I. Muhammad, K.H. Ali, M.M. Ansari, F. ud Din, O.S. Qureshi, K.W. Kim, Y.H. Choe, J.K. Kim, A. Zeb, Simvastatin-loaded solid lipid nanoparticles for enhanced anti-hyperlipidemic activity in hyperlipidemia animal model, International Journal of Pharmaceutics. 560 (2019) 136–143. https://doi.org/10.1016/j.ijpharm.2019.02.002.

[13] H. Mu, R. Holm, Solid lipid nanocarriers in drug delivery: characterization and design, Expert Opinion on Drug Delivery. 15 (2018) 771–785. https://doi.org/10.1080/17425247.2018.1504018.

[14] B.J. Boyd, C.A.S. Bergström, Z. Vinarov, M. Kuentz, J. Brouwers, P. Augustijns, M. Brandl, A. Bernkop-Schnürch, N. Shrestha, V. Préat, A. Müllertz, A. Bauer-Brandl, V. Jannin, Successful oral delivery of poorly water-soluble drugs both depends on the intraluminal behavior of drugs and of appropriate advanced drug delivery systems, European Journal of Pharmaceutical Sciences. 137 (2019) 104967. https://doi.org/10.1016/j.ejps.2019.104967.

[15] J. Desai, H. Thakkar, Effect of particle size on oral bioavailability of darunavir-loaded solid lipid nanoparticles, Taylor & Francis, 2016. https://doi.org/10.1080/02652048.2016.1245363.

[16] K.M. Hosny, B.M. Aljaeid, Sildenafil citrate as oral solid lipid nanoparticles: A novel formula with higher bioavailability and sustained action for treatment of erectile dysfunction, Expert Opinion on Drug Delivery. 11 (2014) 1015–1022. https://doi.org/10.1517/17425247.2014.912212.

[17] N.T. Pandya, P. Jani, J. Vanza, H. Tandel, Solid lipid nanoparticles as an efficient drug delivery system of olmesartan medoxomil for the treatment of hypertension, Colloids and Surfaces B: Biointerfaces. 165 (2018) 37–44. https://doi.org/10.1016/j.colsurfb.2018.02.011.

[18] A. Larsen, R. Holm, M.L. Pedersen, A. Müllertz, Lipid-based formulations for danazol containing a digestible surfactant, labrafil M2125CS: In vivo bioavailability and dynamic in vitro lipolysis, Pharmaceutical Research. 25 (2008) 2769–2777. https://doi.org/10.1007/s11095-008-9641-0.

[19] S.D. Siqueira Jørgensen, M. Al Sawaf, K. Graeser, H. Mu, A. Müllertz, T. Rades, The ability of two in vitro lipolysis models reflecting the human and rat gastro-intestinal conditions to predict the in vivo performance of SNEDDS dosing regimens, European Journal of Pharmaceutics and Biopharmaceutics. 124 (2018) 116–124. https://doi.org/10.1016/j.ejpb.2017.12.014.

[20] K. Patel, S. Padhye, M. Nagarsenker, Duloxetine HCl lipid nanoparticles: preparation, characterization, and dosage form design, AAPS PharmSciTech. 13 (2012) 125–133. https://doi.org/10.1208/s12249-011-9727-6.

[21] K. Elbrink, S. Van Hees, R. Chamanza, D. Roelant, R. Holm, F. Kiekens, Application of solid lipid nanoparticles as a long-term drug delivery platform for intramuscular and subcutaneous administration : in vitro and in vivo evaluation, European Journal of Pharmaceutics and Biopharmaceutics. (2021). https://doi.org/10.1016/j.ejpb.2021.04.004.

[22] I.A. Elbahwy, H.M. Ibrahim, H.R. Ismael, A.A. Kasem, Enhancing bioavailability and controlling the release of glibenclamide from optimized solid lipid nanoparticles, Journal of Drug Delivery Science and Technology. 38 (2017) 78–89. https://doi.org/https://doi.org/10.1016/j.jddst.2017.02.001.

[23] G.A. Shazly, S. Alshehri, M.A. Ibrahim, H.M. Tawfeek, J.A. Razik, Y.A. Hassan, F. Shakeel, Development of Domperidone Solid Lipid Nanoparticles: In Vitro and In Vivo Characterization, AAPS PharmSciTech. 19 (2018) 1712–1719. https://doi.org/10.1208/s12249-018-0987-2.

[24] G. Abdelbary, R.H. Fahmy, Diazepam-loaded solid lipid nanoparticles: design and characterization, AAPS PharmSciTech. 10 (2009) 211–219. https://doi.org/10.1208/s12249-009-9197-2.

[25] S. Baboota, S. Faiyaz, A. Ahuja, J. Ali, S. Shafiq, S. Ahmad, Development and validation of a stability-indicating HPLC method for analysis of celecoxib (CXB) in bulk drug and microemulsion formulations, Acta Chromatographica. 18 (2007) 116–129.

[26] R.H. Müller, K. Mäder, S. Gohla, Solid lipid nanoparticles (SLN) for controlled drug delivery - A review of the state of the art, European Journal of Pharmaceutics and Biopharmaceutics. 50 (2000) 161–177. https://doi.org/10.1016/S0939-6411(00)00087-4.

[27] Y. Lv, H. He, J. Qi, Y. Lu, W. Zhao, X. Dong, W. Wu, Visual validation of the measurement of entrapment efficiency of drug nanocarriers, International Journal of Pharmaceutics. 547 (2018) 395–403. https://doi.org/https://doi.org/10.1016/j.ijpharm.2018.06.025.

[28] A. Baán, P. Adriaensens, J. Lammens, R. Delgado Hernandez, W. Vanden Berghe, L. Pieters, C. Vervaet, F. Kiekens, Dry amorphisation of mangiferin, a poorly water-soluble compound, using mesoporous silica, European Journal of Pharmaceutics and Biopharmaceutics. 141 (2019) 172–179. https://doi.org/10.1016/j.ejpb.2019.05.026.

[29] Á. Juhász, D. Ungor, K. Berta, L. Seres, E. Csapó, Spreadsheet-based nonlinear analysis of in vitro release properties of a model drug from colloidal carriers, Journal of Molecular Liquids. 328 (2021). https://doi.org/10.1016/j.molliq.2021.115405.

[30] L.S. Koester, G.G. Ortega, P. Mayorga, V.L. Bassani, Mathematical evaluation of in vitro release profiles of hydroxypropylmethylcellulose matrix tablets containing carbamazepine associated to β-cyclodextrin, European Journal of Pharmaceutics and Biopharmaceutics. 58 (2004) 177–179. https://doi.org/10.1016/j.ejpb.2004.03.017.

[31] P. Costa, J.M. Sousa Lobo, Modeling and comparison of dissolution profiles, European Journal of Pharmaceutical Sciences. 13 (2001) 123–133. https://doi.org/10.1016/S0928-0987(01)00095-1.

583 [32] J.B. Dressman, C. Reppas, In vitro-in vivo correlations for lipophilic, poorly water-soluble drugs,
584 European Journal of Pharmaceutical Sciences. 11 (2000) 73–80. https://doi.org/10.1016/S0928-
585 0987(00)00181-0.

586 [33] F. Langenbucher, Numerical convolution/deconvolution as a tool for correlating in vitro with in vivo drug
587 availability, Pharmazeutische Industrie. 44 (1982) 1166–1172.

588 [34] L. Bønløkke, L. Hovgaard, H.G. Kristensen, L. Knutson, A. Lindahl, H. Lennernäs, A comparison between
589 direct determination of in vivo dissolution and the deconvolution technique in humans, European Journal
590 of Pharmaceutical Sciences. 8 (1999) 19–27. https://doi.org/10.1016/S0928-0987(98)00055-4.

591 [35] L.J. Henze, B.T. Griffin, M. Christiansen, C. Bundgaard, P. Langguth, R. Holm, Exploring gastric
592 emptying rate in minipigs: Effect of food type and pre-dosing of metoclopramide, European Journal of
593 Pharmaceutical Sciences. 118 (2018) 183–190. https://doi.org/10.1016/j.ejps.2018.03.017.

594 [36] ICH Topic Q 1 A (R2) Stability Testing of new Drug Substances and Products, (2003).
595 https://www.ema.europa.eu/en/documents/scientific-guideline/ich-q-1-r2-stability-testing-new-drug-
596 substances-products-step-5_en.pdf.

597 [37] O.S. Qureshi, A. Zeb, M. Akram, M.S. Kim, J.H. Kang, H.S. Kim, A. Majid, I. Han, S.Y. Chang, O.N.
598 Bae, J.K. Kim, Enhanced acute anti-inflammatory effects of CORM-2-loaded nanoparticles via sustained
599 carbon monoxide delivery, European Journal of Pharmaceutics and Biopharmaceutics. 108 (2016) 187–
600 195. https://doi.org/10.1016/j.ejpb.2016.09.008.

601 [38] N. Dudhipala, K. Veerabrahma, Improved anti-hyperlipidemic activity of Rosuvastatin Calcium via lipid
602 nanoparticles: Pharmacokinetic and pharmacodynamic evaluation, European Journal of Pharmaceutics and
603 Biopharmaceutics. 110 (2017) 47–57. https://doi.org/10.1016/j.ejpb.2016.10.022.

604 [39] E. Angela, C.M.O. Driscoll, M. Mcallister, N. Fotaki, European Journal of Pharmaceutical Sciences
605 Gastrointestinal diseases and their impact on drug solubility : Crohn ' s disease, 152 (2020).
606 https://doi.org/10.1016/j.ejps.2020.105459.

607 [40] N.T. Pandya, P. Jani, J. Vanza, H. Tandel, Solid lipid nanoparticles as an efficient drug delivery system of
608 olmesartan medoxomil for the treatment of hypertension, Colloids and Surfaces B: Biointerfaces. 165
609 (2018) 37–44. https://doi.org/10.1016/j.colsurfb.2018.02.011.

610 [41] A.M. Fatouh, A.H. Elshafeey, A. Abdelbary, Intranasal agomelatine solid lipid nanoparticles to enhance
611 brain delivery: Formulation, optimization and in vivo pharmacokinetics, Drug Design, Development and
612 Therapy. 11 (2017) 1815–1825. https://doi.org/10.2147/DDDT.S102500.

613 [42] A. Zeb, O.S. Qureshi, H.S. Kim, M.S. Kim, J.H. Kang, J.S. Park, J.K. Kim, High payload itraconazole-
614 incorporated lipid nanoparticles with modulated release property for oral and parenteral administration,
615 Journal of Pharmacy and Pharmacology. 69 (2017) 955–966. https://doi.org/10.1111/jphp.12727.

616 [43] A.K. Sharma, P.K. Sahoo, D.K. Majumdar, N. Sharma, R.K. Sharma, A. Kumar, Fabrication and
617 evaluation of lipid nanoparticulates for ocular delivery of a COX-2 inhibitor, Drug Delivery. 23 (2016)
618 3364–3373. https://doi.org/10.1080/10717544.2016.1183720.

619 [44] H.A. Fathi, A. Allam, M. Elsabahy, G. Fetih, M. El-Badry, Nanostructured lipid carriers for improved oral
620 delivery and prolonged antihyperlipidemic effect of simvastatin, Colloids and Surfaces B: Biointerfaces.
621 162 (2018) 236–245. https://doi.org/10.1016/j.colsurfb.2017.11.064.

622 [45] Y.H. Liu, C.S. Sun, Y.R. Hao, T.Y. Jiang, L. Zheng, S.L. Wang, Mechanism of Dissolution Enhancement
623 and Bioavailability of Poorly Water Soluble Celecoxib by Preparing Stable Amorphous Nanoparticles,
624 Journal of Pharmacy and Pharmaceutical Sciences. 13 (2010) 589–606. https://doi.org/Doi
625 10.18433/J3530j.

626 [46] V.V. Kumar, D. Chandrasekar, S. Ramakrishna, V. Kishan, Y.M. Rao, P.V. Diwan, Development and
627 evaluation of nitrendipine loaded solid lipid nanoparticles: Influence of wax and glyceride lipids on plasma
628 pharmacokinetics, International Journal of Pharmaceutics. 335 (2007) 167–175.
629 https://doi.org/https://doi.org/10.1016/j.ijpharm.2006.11.004.

630 [47] R. Olaughlin, C. Sachs, H. Brittain, E. Cohen, P. Timmins, S. Varia, Effects of Variations in
631 Physicochemical Properties of Glyceryl Monostearate on the Stability of an Oil-in-Water Cream, J Soc
632 Cosmet Chem. 40 (1989) 215–229.

633 [48] E.D.P. Almeida, A.A. Costa, M.R. Serafini, F.C. Rossetti, J.M. Marchetti, V.H. V. Sarmento, R. De S.
634 Nunes, M.E.G. Valerio, A.A.S. Araújo, A.A.M. Lira, Preparation and characterization of chloroaluminum

phthalocyanine-loaded solid lipid nanoparticles by thermal analysis and powder X-ray diffraction techniques, Journal of Thermal Analysis and Calorimetry. 108 (2012) 191–196. https://doi.org/10.1007/s10973-011-1868-z.

[49] N. Dudhipala, K. Veerabrahma, Candesartan cilexetil loaded solid lipid nanoparticles for oral delivery: Characterization, pharmacokinetic and pharmacodynamic evaluation, Drug Delivery. 23 (2016) 395–404. https://doi.org/10.3109/10717544.2014.914986.

[50] P. Nirbhavane, N. Vemuri, N. Kumar, G.K. Khuller, Lipid Nanocarrier-Mediated Drug Delivery System to Enhance the Oral Bioavailability of Rifabutin, AAPS PharmSciTech. 18 (2017) 829–837. https://doi.org/10.1208/s12249-016-0559-2.

[51] E.S. Ha, G.H. Choo, I.H. Baek, M.S. Kim, Formulation, characterization, and in vivo evaluation of celecoxib-PVP solid dispersion nanoparticles using supercritical antisolvent process, Molecules. 19 (2014) 20325–20339. https://doi.org/10.3390/molecules191220325.

[52] F. Langenbucher, Letters to the Editor: Linearization of dissolution rate curves by the Weibull distribution, Journal of Pharmacy and Pharmacology. 24 (1972) 979–981. https://doi.org/10.1111/j.2042-7158.1972.tb08930.x.

[53] Y.M. Yin, F. De Cui, C.F. Mu, M.K. Choi, J.S. Kim, S.J. Chung, C.K. Shim, D.D. Kim, Docetaxel microemulsion for enhanced oral bioavailability: Preparation and in vitro and in vivo evaluation, Journal of Controlled Release. 140 (2009) 86–94. https://doi.org/10.1016/j.jconrel.2009.08.015.

[54] T.H. Tran, T. Ramasamy, D.H. Truong, B.S. Shin, H.G. Choi, C.S. Yong, J.O. Kim, Development of vorinostat-loaded solid lipid nanoparticles to enhance pharmacokinetics and efficacy against multidrug-resistant cancer cells, Pharmaceutical Research. 31 (2014) 1978–1988. https://doi.org/10.1007/s11095-014-1300-z.

[55] H.H. Holzer, C.M. Turkelson, T.E. Solomon, H.E. Raybould, Intestinal lipid inhibits gastric emptying via CCK and a vagal capsaicin- sensitive afferent pathway in rats, American Journal of Physiology - Gastrointestinal and Liver Physiology. 267 (1994). https://doi.org/10.1152/ajpgi.1994.267.4.g625.

[56] F. Ud Din, J.Y. Choi, D.W. Kim, O. Mustapha, D.S. Kim, R.K. Thapa, K. Sae, Y.S. Ku, K.T. Youn, S. Oh, J. Yong, K. Oh, H.-G. Choi, U. Din, S.K. Ku, Y.S. Youn, K.T. Oh, C.S. Yong, J.O. Kim, Drug Delivery Irinotecan-encapsulated double-reverse thermosensitive nanocarrier system for rectal administration Irinotecan-encapsulated double-reverse thermosensitive nanocarrier system for rectal administration, Drug Deliv. 24 (2017) 502–510. https://doi.org/10.1080/10717544.2016.1272651.

[57] R. Tiwari, K. Pathak, Nanostructured lipid carrier versus solid lipid nanoparticles of simvastatin: Comparative analysis of characteristics, pharmacokinetics and tissue uptake, International Journal of Pharmaceutics. 415 (2011) 232–243. https://doi.org/10.1016/j.ijpharm.2011.05.044.

Figure Captions

Fig. 1A. DSC thermograms of drug-free solid lipid nanoparticles (pink), CCX-1 (green), CCX-2 (red), GMS (blue), and plain celecoxib (brown).

Fig. 1B. X-ray powder diffraction patterns of CCX-1 (green), CCX-2 (dark blue), drug-free solid lipid nanoparticles (brown), plain celecoxib (blue), and GMS (purple).

Fig. 2. *In vitro* drug release profiles per formulation; (A) CCX-1; (B) CCX-2; (C) plain celecoxib. Data are expressed as the mean ± SD (n = 3).

Fig. 3. *In vitro* drug release profiles per medium; (A) SGF; (B) FeSSIF; (C) FaSSIF. Data are expressed as the mean ± SD (n = 3).

Fig. 4. Comparison of R^2 values qualifying the result of nonlinear dissolution models on different formulations.

Fig. 5. (A) Plasma concentration-time profiles for the SLN formulations and celecoxib reference after oral administration to rats (mean profiles ± SD, n = 6). (B) Mean deconvolution profiles of the SLN formulations and the celecoxib reference (n = 6).

690 **Table 1** Composition of the prepared SLN formulations

Components	Formulation codes		
	CCX-1	CCX-2	Blanco
CCX (mg/g)	4.108	20.000	-
GMS (g/g)	0.100	0.100	0.100
Tween 80 extra pure (g/g)	0.010	0.010	0.010
Sodium deoxycholate (g/g)	0.005	0.005	0.005
Ultrapure water (g/g)	0.881	0.865	0.885

691

692 **Table 2** Characterization of the different formulations: zeta potential, particle size, entrapment
693 efficiency, and loading capacity (n=3 with standard deviation)

Formulation	ZP (mV)	Dx(50) (nm)	EE (%)	LC (%)
CCX-1	-43.90 ± 0.53	39.80 ± 0.53	96.95 ± 0.02	3.88 ± 0.04
CCX-2	-44.60 ± 1.59	91.47 ± 0.90	99.44 ± 0.00	19.78 ± 0.03
Blanco	-47.90 ± 2.15	19.67 ± 0.46	-	-

694

695 **Table 3** Determination coefficient (R^2), scale (a), and shape (b) parameters for the Weibull
696 model

	FaSSIF			FeSSIF			SGF		
	CCX	CCX-1	CCX-2	CCX	CCX-1	CCX-2	CCX	CCX-1	CCX-2
R^2	0.9405	0.9862	0.9289	0.9911	0.9964	0.9633	0.9615	0.9738	0.8890
a	0.1904	0.0013	0.1044	0.0365	0.0001	0.0060	0.0572	0.0028	0.1079
b	0.2637	1.2792	0.3391	0.5396	1.5111	0.7607	0.3878	1.0362	0.3219

697

Table 4 Pharmacokinetic parameters of celecoxib in rats following oral administration (mean values for n = 6 with standard deviation)

Analyte	**Celecoxib**		
Formulation	**CCX-1**	**CCX-2**	**CCX-3**
Dosing route	**PO**	**PO**	**PO**
Dose (mg/mL)	3	3	3
n	6	6	6
C_0 (ng/mL)	-	-	-
T_{last} (h)	30	30	30
$T_{1/2}$ (h)	3.29 ± 0.38	3.56 ± 0.33	3.45 ± 0.88
t_{max} (h)	2.67 ± 1.03	3.33 ± 1.03	2.17 ± 0.98
C_{max} (ng/mL)	7106.67 ± 1133.94	4283.33 ± 897.97	2746.67 ± 167.89
C_{max}/dose (ng/mL)	2368.89	1427.78	915.56
AUC_{0-t} (ng.h/mL)	46790.60 ± 9752.74	33964.13 ± 7058.02	18620.97 ± 2659.02
AUC_{0-inf} (ng.h/mL)	46926.90 ± 9783.33	34115.92 ± 7086.55	18852.62 ± 2424.47
AUC/Dose (ng.h/mL)	15642.30	11371.97	6284.21
MRT (h)	5.44 ± 0.82	6.32 ± 0.88	5.17 ± 0.86
F_{0-t}	251%	182%	100%
F_{0-inf}	249%	181%	100%

701 **Table 5** Average deconvolution time points (h) following oral administration of celecoxib
702 (mean values for n = 6)

Absorbed fraction (%)	CCX-1 (h)	CCX-2 (h)	CCX-3 (h)
10	0.5	0.7	0.2
50	2.6	3.4	2.3
90	12.0	13.4	11.5

703

704

SUPPLEMENTARY DATA

The influence on the oral bioavailability of solubilized and suspended drug in a lipid nanoparticle formulation: in vitro and in vivo evaluation

Figure A.1

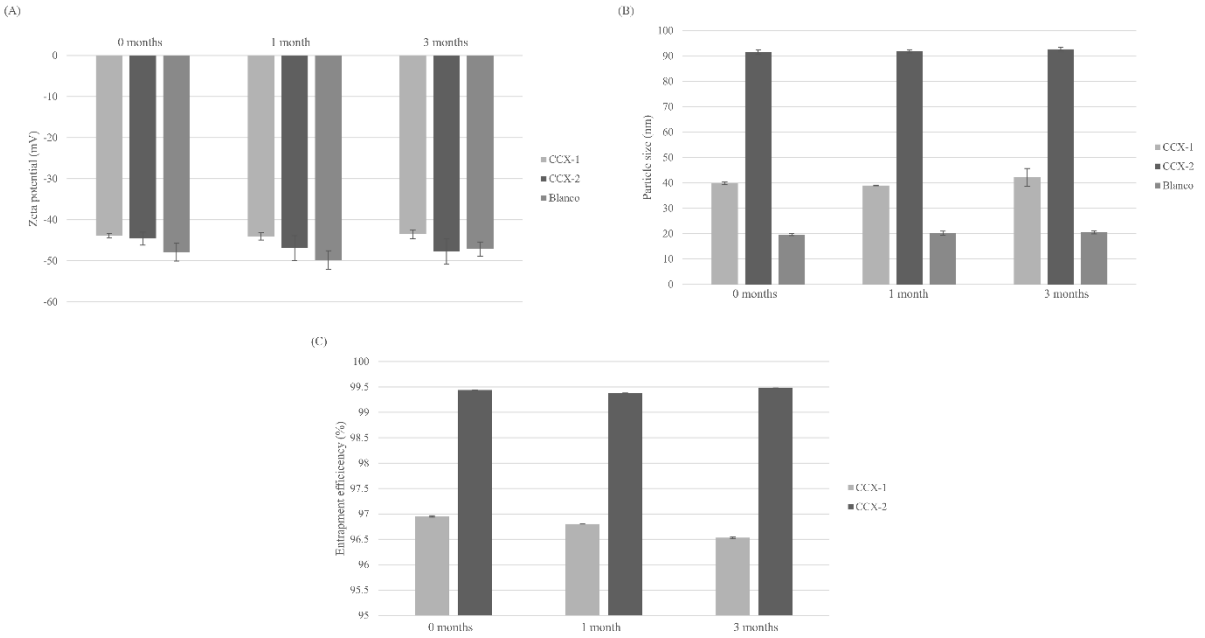

Storage stability data of the drug-free and drug-loaded SLNs at 4°C (mean values ± SD, n = 3); (A) zeta potential; (B) particle size; (C) entrapment efficiency.

713 **Table A.1**

0 months	ZP (mV)	Dx(50) (nm)	EE (%)
CCX-1	-43.9 ± 0.529	39.8 ± 0.529	96.95 ± 0.015
CCX-2	-44.6 ± 1.587	91.5 ± 0.902	99.44 ± 0.004
Blanco	-47.9 ± 2.152	19.7 ± 0.458	-
1 month	ZP (mV)	Dx(50) (nm)	EE (%)
CCX-1	-44 ± 0.929	39.0 ± 0.153	96.80 ± 0.001
CCX-2	-46.9 ± 3.055	91.9 ± 0.636	99.38 ± 0.001
Blanco	-49.8 ± 2.290	20.2 ± 0.778	-
3 months	ZP (mV)	Dx(50) (nm)	EE (%)
CCX-1	-43.5 ± 1.050	42.2 ± 3.523	96.53 ± 0.012
CCX-2	-47.7 ± 3.083	92.7 ± 0.707	99.48 ± 0.001
Blanco	-47.1 ± 1.721	20.5 ± 0.566	-

714

715 Storage stability data of the drug-free and drug-loaded formulations at 4°C: zeta potential,
716 particle size, and entrapment efficiency (mean values ± SD, n=3).